

# Gravity change observed in a local gravity network and its implication to seasonal precipitation in Dali county, Yunnan province, China

Xin Zhou · Wenke Sun · Hui Li · Shuhei Okubo ·  
Shaoan Sun · Lelin Xing · Dongzhi Liu ·  
Chongyang Shen

Received: 21 August 2013 / Accepted: 20 November 2013 / Published online: 10 December 2013

© The Seismological Society of China, Institute of Geophysics, China Earthquake Administration and Springer-Verlag Berlin Heidelberg 2013

**Abstract** This study investigates data-processing methods and examines the precipitation effect on gravity measurements at the Dali gravity network, established in 2005. High-quality gravity data were collected during four measurement campaigns. To use the gravity data validly, some geophysical corrections must be considered carefully. We first discuss data-processing methods using weighted least-squares adjustment with the constraint of the absolute gravity datum. Results indicate that the gravity precision can be improved if all absolute gravity data are used as constraints and if calibration functions of relative gravimeters are modeled within the observation function. Using this data-processing scheme, the mean point gravity precision is better than 12  $\mu\text{gal}$ . After determining the best data-processing scheme, we then process the gravity data obtained in the four measurement campaigns, and obtain gravity changes in three time periods. Results show that the gravity has a remarkable change of more than 50  $\mu\text{gal}$  in the first time period from Apr–May of 2005 to Aug–Sept of 2007. To interpret the large gravity change, a mean water mass change (0.6 m in height) is assumed in the ETOPO1 topographic model. Calculations of the precipitation effect on gravity show that it can reach the same order of the

observed gravity change. It is regarded as a main source of the remarkable gravity change in the Dali gravity network, suggesting that the precipitation effect on gravity measurements must be considered carefully.

**Keywords** Gravity network · Gravity change · Gravity datum · Weighted constraint · Precipitation effect

## 1 Introduction

The Red River fault zone (RRFZ), situated east of the San Jiang fault zone in western Yunnan, is the boundary between the South China block and the Indochina block. It is a geological discontinuity from northwestern to southeastern Yunnan province together with the Ailao Shan fault zone (Leloup et al. 1995). The fault extends about 1,000 km through the continent from Eryuan in the northern Dali area to northern Vietnam through the Dali, Yuanjiang, and Honghe areas (Hao et al. 2005).

The Red River fault's tectonic activity is complicated; its new tectonic movement is remarkable. It corresponds to a great left-lateral strike-slip shear fault between 23.4–13.7 Ma BP and changes to a large-scale right-lateral strike-slip shear fault 13.7 Ma BP (Xiang et al. 2007). It is generally divided into three segments in terms of the fault activity characteristics—the north, the middle, and the south—with a marked difference among regions. The north segment, situated between Eryuan and Midu, including the Erhai fault, Fushouchang fault, etc., corresponds to a right-lateral fault with tensile-shear activity characteristics. The activity characteristics of the middle segment are horizontal shear from Midu to Yuanchun. The south segment conforms to a strike-slip fault with right-lateral motion

X. Zhou · W. Sun (✉)

Laboratory of Computational Geodynamics, University of Chinese Academy of Sciences, Beijing, China  
e-mail: sunw@ucas.ac.cn

H. Li · S. Sun · L. Xing · D. Liu · C. Shen

Institute of Seismology, China Earthquake Administration, Wuhan, China

S. Okubo

Earthquake Research Institute, The University of Tokyo, Tokyo, Japan

feature. However, the seismicity of the north segment appears to be much more intense, with higher frequency and greater magnitude than those of the south segment. During the 527 years from 1481 to 2008, 17 earthquakes of magnitude greater than  $M6$  struck this area. The situation in the south segment differed: no earthquake was stronger than magnitude 6, and fewer  $M4$ – $M5$  earthquakes occurred throughout its history. Zhao (1995) inverted the active fault characteristic of RRFZ using gravity variation data and GPS data and derived the same result as that obtained from seismicity and geology, showing that horizontal displacement field movement mainly concentrated at the north segment. The RRFZ attracts scientists' attention because of its specific tectonic geology and geodynamics in the southern Tibetan Plateau.

To investigate crustal deformation, tectonic movement and fault activity in the northern RRFZ area in Dali county, known as the Western Yunnan Earthquake Prediction Experimental Area (Wang et al. 1989), a joint research project was undertaken in 2005 by the Institute of Seismology (IOS), China Earthquake Administration (CEA) and Earthquake Research Institute (ERI), The University of Tokyo, Japan. The project, including four absolute gravity stations and 64 relative gravity sites, is intended to establish a high-precision gravity network to study the RRFZ fault activity through gravity.

This gravity network has been reoccupied by four measurement campaigns since 2005, of which three campaigns were controlled by absolute gravity measurements. One campaign was made solely by relative gravity measurement. The gravity data collected in the four campaigns are generally reliable, and the gravity changes derived from the repeated measurements are useful in studying crustal density variation, tectonic movement, seismic activity, and so on. However, before applying gravity data in geophysical problems, proper data processing is necessary. Especially, some physical corrections such as the precipitation effect must be considered carefully.

Any change in precipitation, moisture, or water storage in the aquifer must result in water mass redistribution. Therefore, gravity changes correspondingly (Torge 1989; Kazama and Okubo 2009). A water mass change can be represented by an infinite plate layer (Bouguer layer) in a flat region. However, if gravity sites are located in a mountainous area, the corresponding terrain height must be considered. Jia et al. (1995) studied relative gravity data by considering the hydrological effect. They claimed that the gravity disturbance might reach about 10–20  $\mu\text{gal}$  because of the surface water in the Dali region. Imanishi et al. (2006) applied a tank model to investigate the transient gravity distribution induced by hydrological factors over several days. They found that a linear gravity response to precipitation is  $-0.04 \mu\text{gal}/\text{mm}$ , and that it increases

constantly by 0.26  $\mu\text{gal}/\text{day}$  after rainfall. Kazama and Okubo (2009) considered the gravity variation caused by a 3-D time-dependent groundwater disturbance model. Then they discovered that the most dominant gravity effect occurs in a region with 150 m radius distance from the observation point through investigation using a nonlinear diffusion equation and analyzing gravity observation data. Boy and Hinderer (2006), considering a global hydrological model, reported that the largest amplitude of seasonal gravity variation is about 50  $\mu\text{gal}$ .

As described in this paper, we first explain data-processing methods for the Dali gravity network constrained with absolute gravity data; then we discuss how to use the data and calibration functions of a relative gravimeter in adjustment. After determining the best data-processing scheme, we process the gravity data obtained during the four measurement campaigns. Thereby, we obtain gravity changes in three time periods. Results showed that the gravity has a remarkable change in the first time period. To interpret the large gravity change, a mean water mass model is assumed for storage in the ETOPO1 topographic model. The precipitation effect on gravity is calculated. Results show that the precipitation effect is a main reason for the remarkable gravity change.

## 2 Gravity observation at the Dali gravity network

The gravity network established through the joint research program between IOS and ERI is located in the Dali area of Yunnan province, at the eastern margin of Tibetan Plateau. The network includes 4 absolute gravimetric stations and 64 relative observation points (Fig. 1). The absolute stations were chosen as (1) the observation cave of the Western Yunnan Earthquake Prediction Experimental Area (Xiaguan), (2) the observation cave of Midu Seismostation (Midu), (3) the observation room of Eryuan Seismostation (Eryuan), and (4) the observation room of Jianchuan Seismostation (Jianchuan). The Xiaguan, Midu, and Jianchuan stations have stable observation conditions with low ambient noise. High-quality gravity data were obtained at these stations. The environmental conditions at Eryuan station are slightly worse than those at any of the other three absolute stations, but the observed gravity data are satisfactory. In Fig. 1, black circles represent the 64 relative gravimetric points at the Dali gravity network which comprises three loops and several South–North and East–West lines. To control the relative network efficiently, we perform gravity measurements between each absolute station and its surrounding relative gravity points with relative gravimeters at each gravity measurement campaign.

During 2005–2008, four gravity measurement campaigns were performed: from Aug 27 to Sept 12 in 2005,

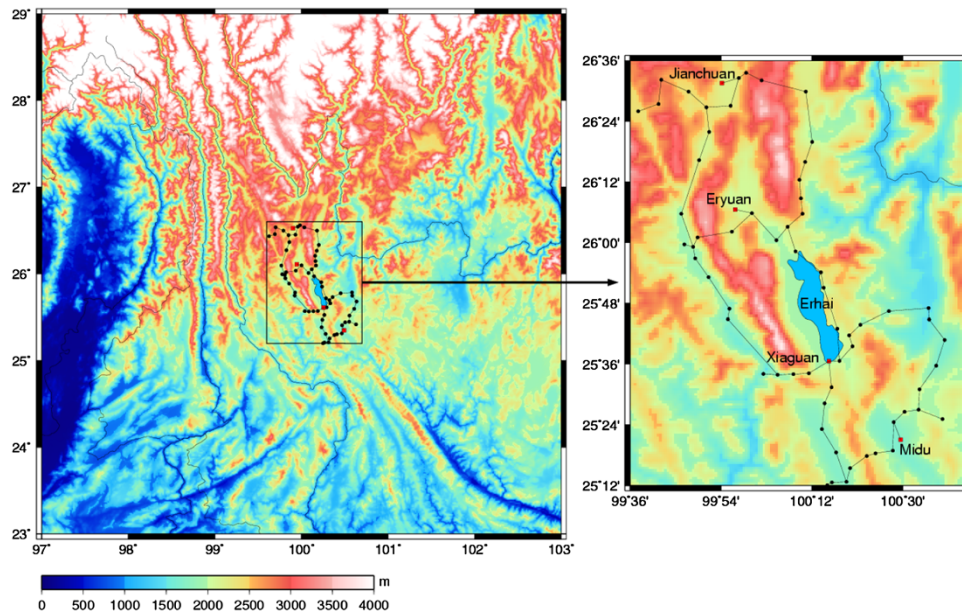


**Fig. 1** Gravity network and topography (ETOPO1) of Dali. *Left red points* represent the four absolute gravity stations Midu, Xiaguan, Eryuan, and Jianchuan; *the black points* represent the relative gravity stations

**Table 1** Observation dates and absolute/relative gravimeters employed at the four gravity measurement campaigns at the Dali gravity network

Campaigns	Observing date	Relative gravimeters (LaCoste and Romberg)	Absolute gravimeters
1	Aug 27–Sept 12, 2005	G581, G793, G854, G1003, G1132	FG5#212(ERI)
2	Apr 27–May 10, 2007	G999, G1027	
3	Nov 23–Dec 2, 2007	G854, G1003, G1134	FG5#232(IOUS)
4	Sept 24–Oct 30, 2008	G793, G853, G854	FG5#232(IOUS)

from Apr 27 to May 10 and from Nov 23 to Dec 2 in 2007, and from Sept 24 to Oct 30 in 2008. Hybrid gravity measurements were conducted during the first, second, and fourth campaigns, i.e., the absolute and relative gravity measurements were performed synchronously. The third campaign lacked absolute gravity measurements because no absolute gravimeter was available. The gravimeters used in the four campaigns are presented in Table 1: two absolute gravimeters FG5 produced by Micro-g LaCoste, Inc. and 9 LaCoste and Romberg (LCR) G-type relative gravimeters were used in the four campaigns. The absolute gravimeter FG5#212 owned by ERI was used in 2005; the absolute gravimeter FG5#232 owned by IOS was used in the third and fourth campaigns. The relative gravimeter LCR #581 belonged to ERI. All other relative gravimeters belongs to IOS. These relative gravimeters were also used to measure the gravity gradients at the four absolute gravity stations. High-quality gravity data were acquired at the four gravity measurement campaigns at the Dali gravity network.

### 3 Data processing for the absolute gravity data

The accuracy of absolute gravimetry is about  $2 \times 10^{-8} \text{ ms}^{-2}$  ( $\mu\text{gal}$ ) at present. According to the results of the second European comparison of absolute gravimeters at Luxembourg by the European Center for Geodynamics and Seismology, systematic errors are small among different FG5 gravimeters (Xing et al. 2009), which implies that although two different absolute gravimeters were used at three repeated gravity measurements at the above network, systematic error can be ignored in the obtained absolute gravity data.

In absolute gravity measurement, a gravity gradient is necessary. For this purpose, we measure the gravity gradient at each absolute gravity station at least six return-measurements with multiple relative gravimeters to guarantee accuracy. The final gravity gradients for the four stations are presented in Table 2.

As shown in Table 2, during the four measurement campaigns, we collected at least 25 sets of absolute gravity data at

**Table 2** Gravity data of the four absolute observation stations

Sites	Date	Drop sets	STD ( $\mu\text{gal}$ )	Gradient ( $\mu\text{gal}/\text{cm}$ )	Gravity at 1.3 m ( $\mu\text{gal}$ )	Gravity on the surface ( $\mu\text{gal}$ )
Midu	2005.09.03	100	1.16	-2.641	978,394,738.7	978,395,082.0
	2007.11.24	25	0.95	-2.640	978,394,745.6	978,395,088.8
	2008.10.26	50	1.10	-2.629	978,394,747.1	978,395,088.9
Xiaguan	2005.09.06	84	0.95	-2.382	978,346,489.6	978,346,799.3
	2007.11.26	25	1.03	-2.344	978,346,485.2	978,346,789.9
	2008.10.27	25	0.79	-2.347	978,346,477.4	978,346,782.5
Eryuan	2005.09.09	49	1.06	-2.510	978,327,741.2	978,328,067.5
	2007.11.28	25	0.80	-2.512	978,327,746.6	978,328,073.2
	2008.11.02	25	1.22	-2.499	978,327,738.1	978,328,063.0
Jianchuan	2005.09.13	37	1.19	-2.710	978,317,085.3	978,317,437.6
	2007.11.30	25	0.73	-2.768	978,317,083.0	978,317,442.8
	2008.10.30	25	0.84	-2.697	978,317,077.4	978,317,428.0

Gravimeter FG5#212 was used in 2005, and FG5#232 was used in 2007 and 2008

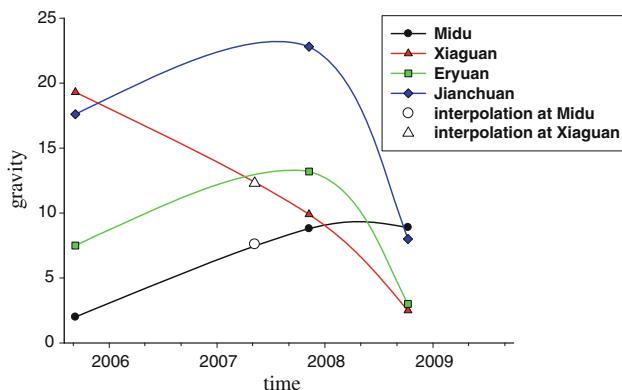


**Fig. 2** Absolute gravity time series at the four gravity stations. *Black line* Midu; *red line* Xiaguan; *green line* Eryuan; *blue line* Jianchuan. The *hollow circle* and *triangle*, respectively, represent the interpolated gravity values in April 2007 at Midu and Xiaguan stations

each gravity station, each set including 100 free-fall drops. A single drop was made at interval of 10 s. In total, 2,500 drops were collected at each station. Then “g” software (developed by Micro-g LaCoste, Inc.) was applied to data processing. The final gravity values were derived after geophysical corrections including those for the tides and their loadings, polar motion, atmospheric pressure effect, and the vertical gravity gradient (Liu et al. 2007). The geophysical correction parameters were obtained from actual data. The absolute gravity observations including standard deviations, sets of drops, valid sets, gravity values at observation height (1.3 m over ground) after geophysical correction (earth tide, ocean tide and polar motion), and gravity values on the earth surface collected in 2005, 2007, and 2008 at four absolute stations, are summarized in Table 2. Table 2 shows that more than 20 sets of gravity data were collected at all stations. The standard deviations are better than 1.25  $\mu\text{gal}$ .

The time series of the observed absolute gravity on the surface at the four gravity stations are depicted in Fig. 2. Figure 2 shows that the gravity at Midu station increases throughout the time period; the gravity at Xiaguan station decreases almost in a linear trend; the gravity at Eryuan and Jianchuan stations have a similar change trend, increasing at the time period of 2005–2007, but decreasing in 2008. These gravity change behaviors will be discussed later.

However, since the third gravity measurement campaign (Apr–May 2007) was conducted only for relative gravity measurements without absolute gravity measurements. To have a reference datum for the relative gravity, we might estimate the absolute gravity values by interpolating the observed absolute gravity in the three measurement campaigns at Xiaguan and Midu stations. The reason to choose the two stations is that the gravity trends are linear and stable. Therefore, the estimated gravity value by interpolation is expected to be stable, with no possible large deviation. Finally, we obtain the estimated absolute gravity values, 978395087.8  $\mu\text{gal}$  for Midu and 978346792.1  $\mu\text{gal}$  for Xiaguan, which are denoted, respectively, as a circle and an hollow triangle in Fig. 2.

## 4 Data processing for relative gravity data

### 4.1 Relative gravity measurement

The precision of gravimeter LCR-G is 10  $\mu\text{gal}$ , with a drift rate of less than  $\pm 5$   $\mu\text{gal}/\text{h}$ . To guarantee the data quality of relative gravimetry, the following measurement scheme was adopted for the Dali gravity network.

- At least 2 LCR-G gravimeters must be used in the relative gravity measurement (more than three

gravimeters were used for the first, third, and fourth campaigns).

- (b) To determine the drift rate of a gravimeter and eliminate the systemic error, a round-trip measurement, such as 1–2–3–...–3–2–1 was used.
- (c) The gravity difference between go-measurements and return-measurements at each station is limited to less than 25  $\mu\text{gal}$  for a single gravimeter. The maximum difference among all gravimeters is expected to be less than 36  $\mu\text{gal}$ .
- (d) Observation time, height over the benchmark, and atmospheric pressure at each site should be recorded correctly.
- (e) The gravimeter must be checked and adjusted to the optimum status every day.
- (f) During a return measurement, if the breaking time is longer than 2 h at a site, a repeat measurement must take place at the last site in the same route.
- (g) The same route should be used in a return measurement to estimate the gravimeter drift rate.

#### 4.2 Observation equation

Preliminary processing for raw data is necessary, i.e., the raw data must be converted to gravity values with the scale table provided by the instrument producer, and the tidal correction, height correction, and air pressure correction should be performed. Then the gravity data must be adjusted further for the whole network. For this purpose, we must consider a reasonable observation equation. Without loss of generality, the observation function for relative gravity difference between two stations  $i$  and  $j$  can be written as

$$\Delta l_{i,j} + v_{i,j} = g_j - g_i + (\Delta F(z_j) - \Delta F(z_i)) + (D(t_j) - D(t_i)), \tag{1}$$

where  $\Delta l_{i,j} = l_j - l_i$  is the relative gravity segment difference between sites  $i$  and  $j$ ,  $v_{i,j}$  is the error of the segment difference,  $g_i$  and  $g_j$  are gravity values at sites  $i$  and  $j$ , respectively;  $\Delta F(z_i)$  and  $\Delta F(z_j)$  are the calibration functions for readings  $z_i$  and  $z_j$ ;  $D(t_i)$  and  $D(t_j)$  are drift functions. The calibration function and the drift function can be modeled as shown below according to Torge (1989).

$$\Delta F(z) = \sum_{n=1}^p b_n z^n + \sum_{n=1}^q (x_n \cos \omega_n z + y_n \sin \omega_n z) \tag{2}$$

$$D(t) = \sum_{m=1}^k d_m (t - t_0)^m \tag{3}$$

In those equations,  $b_n$  is the coefficient of the long-wavelength component of the calibration function,  $x_n$  and  $y_n$  are the coefficients of the periodic component,  $\omega_n$  is the

frequency of the reading  $z$ ,  $p$ , and  $q$  are the degrees,  $d_m$  is the drift parameter,  $t_0$  is the initial time of a baseline, and  $k$  is the degree.

Data processing using Eq. (1) is a classic rank defect least-squares adjustment. An additional pseudo-observation equation must generally be introduced to overcome the rank defect (Hwang et al. 2002). Fortunately, we can avoid the rank defect problem because the absolute gravity of the Dali network can be derived from the three campaigns and data interpolation. Therefore, the absolute gravity datum as a pseudo-observation equation and Eq. (1) constitute a new observation function in which the gravity values and parameters such as drift coefficients and calibration coefficients are estimated using least-squares adjustments with a weighted constraint.

#### 4.3 Data processing for the Dali gravity network

As described above, before applying least-squares adjustment to the gravity network, effects of earth tides, instrument height, and air pressure must be corrected for raw data. We adopt 1.163 as the tidal factor for the four measurement campaigns. The tidal factor is derived from continuous tidal gravity observation at the Kunming seismic station (102°42', 25°03'). The ocean tidal effect seems small (at magnitude of 0.1  $\mu\text{gal}$ ) because the distance from Dali to the nearest coast is more than 800 km. Because all two adjacent gravity sites are within 15 km distance in the Dali network, the drift function can be regarded as the linear change for LCR-G gravimeters (Torge 1989). It can be resolved with gravity values using least-squares inversion.

The linear drift is usually considered in the long-wavelength component of the calibration function. Because of the slow change of the spring as time, the calibration function must change correspondingly. To calibrate the instrument to revising the linear coefficient and periodic coefficients, a calibrating measurement is usually performed in a specified field. In fact, the Dali network can be used to calibrate the LCR gravimeter because we have strong control by the four accurate absolute stations. We adopt the following schemes to process the relative gravity data in the Dali network and to investigate the effect of calibration function in the least-squares adjustment.

*Case 1* For one absolute gravity datum, we model the drift function to one degree without consideration of the calibration function; the last calibration result is used for the linear coefficient. The Xiaguan station is the best one (about 30 m inside the cave and the noise is low) within the four absolute stations. Therefore, we choose the Dali absolute gravity as the constraint datum. Table 2 shows that the maximum STD is only 1.03  $\mu\text{gal}$  (Table 3).

*Case 2* As in Case 1, but the two absolute gravity stations at Dali and Midu are used as weighted constraint data.

**Table 3** Relative gravity data processing schemes

Cases	Absolute gravity datum number	Calibration function estimation	
		Long-wavelength component	Periodic components
Case 1	1 (Xiaguan)	No	No
Case 2	2 (Xiaguan and Midu)	No	No
Case 3	4 (All stations)	No	No
Case 4	4 (All stations)	Yes	No
Case 5	4 (All stations)	Yes	Yes

**Table 4** Linear coefficients of long wavelength of relative gravimeter's calibration functions used in Case 1, Case 2, and Case 3

LCR gravimeter	Linear coefficient	LCR Gravimeter	Linear coefficient
G581	1.000105	G793	1.000541
G854	1.000543	G1003	1.000510
G1132	1.000779	G999	1.000657
G1027	1.000868	G1134	1.000426
G853	1.000341		

*Case 3* As in Case 1, but all four absolute gravity stations are used as weighted constraints.

*Case 4* We use the four absolute gravity measurements and model the linear long-wavelength component of calibration function and drift function to degree one.

*Case 5* We use the four absolute gravity measurements and model the linear long-wavelength and periodic components of calibration function and drift function to degree one, where four periods of the LCR-G gravimeter are used: 36.7, 73.3, 100, and 220.

We summarize above relative gravity data-processing schemes in Table 3. It is worthy to note that two absolute gravity stations at Xiaguan and Midu are used as weighted constraints for gravity measurements during Apr–May, 2007. The linear coefficients of the last calibration used in Cases 1–3 are presented in Table 4.

In Cases 1–3, we used the STD values presented in Table 2 as the prior accuracy of the weighted constraints. The unit-weighted error of the total reliable gravity data is set to 15  $\mu\text{gal}$ . That of a signal gravimeter is set initially to 15  $\mu\text{gal}$ . When the first round adjustment is completed, we must remove the outliers, with the following condition: if the difference between the go-measurements and return-measurements exceeds 25  $\mu\text{gal}$  at the same segment for a single gravimeter, or if the maximum difference of all gravimeters is larger than 30  $\mu\text{gal}$ , then the posterior variance is used as the prior variance for the next adjustment. However, the prior information of the absolute datum retains the initial setting. We repeat the steps described

above until the posterior and prior variance are nearly equal. In Case 4, we resolve the linear coefficient of the long wavelength of the calibration function and substitute it for Table 4 first. In Case 5, we also resolve the long wavelength and periodic components first. We then repeat the same work as described above to resolve the gravity values at each station.

#### 4.4 Final gravity results

Using the schemes presented above, we process the observed gravity data for the five cases. Then we obtain the final results in gravity accuracy analysis, respectively. In all cases, the conditions are satisfied. The segment differences for a gravimeter are all smaller than 25  $\mu\text{gal}$ . The maximum segment differences among the gravimeters are all less than 30  $\mu\text{gal}$  after weighted constraint adjustment. Then we compared the results (Table 5) to determine the best method or scheme. For that purpose, the mean point value precision used to measure the adjustment result is portrayed in Table 5 for Cases 1–5. The results of Cases 1–3 show that the more absolute data are employed, the better the accuracy derived when the calibration function is not regarded as an unknown parameter of adjustment equation. The results of Cases 3–5 reflect that the accuracy for modeling the long wavelength and periodic components is better than that without considering the same weighted constraints. Case 5 yields the best accuracy among all schemes, indicating that this scheme is an effective model, especially for an inaccurate calibration function of the LCR-G gravimeter. Furthermore, derivation of more accurate calibration function necessitates the use of more go-measurements and return-measurements.

The mean point accuracy of the second and third campaigns is better than 9  $\mu\text{gal}$ , but the fourth campaign is 21.4  $\mu\text{gal}$  in Case 1. The results imply that a gravity change larger than 65  $\mu\text{gal}$  (i.e., three times larger than the sigma) is expected to be detectable with confidence of 99.7 %. For cases 3–5, a gravity change greater than 30  $\mu\text{gal}$  is expected to be detected.

**Table 5** Mean point gravity precision after weighted-constraints least-squares adjustment. Unit:  $\mu\text{gal}$ 

Campaign	Period	Case 1	Case 2	Case 3	Case 4	Case 5
1	Aug 27–Sept 12, 2005	14.3	12.7	8.8	8.4	7.2
2	Apr 27–May 10, 2007	8.1	7.2	–	7.2	6.4
3	Nov 23–Dec 2, 2007	8.4	7.6	5.6	5.5	5.1
4	Sept 24–Oct 30, 2008	21.4	19.2	13.9	11.3	10.4

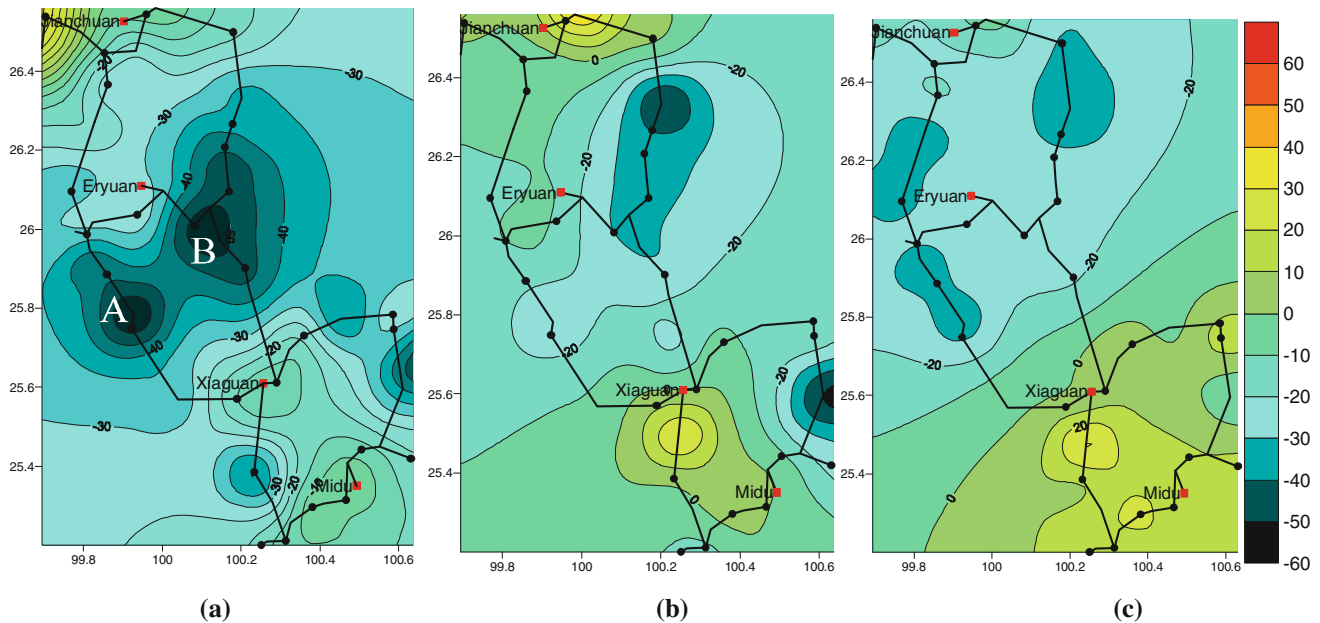


**Fig. 3** Gravity change distribution of the Dali gravity network, obtained for the time periods of (a) Apr 27–May 10, 2007 and Aug 27–Sept 12, 2005, (b) Nov 23–Dec 2, 2007 and Aug 27–Sept 12, 2005, and (c) Sept 24–Oct 30, 2008 and Aug 27–Sept 12, 2005. Unit:  $\mu\text{gal}$

Taking the gravity obtained in the first measurement campaign (Aug 27–Sept 12, 2005) as the reference, we obtain gravity changes of the second, the third, and the fourth (Apr 27–May 10, 2007, Nov 23–Dec 2, 2007, and Sept 24–Oct 30, 2008) measurement campaigns using the results of Case 5. The gravity change distributions for the three time periods are depicted in Figs. 3a, b, and c, respectively. Figure 3a shows two areas, A and B, with marked negative gravity changes of more than  $50 \mu\text{gal}$ . Each is located between the absolute gravity stations Xiaoguan and Eryuan. The gravity changes for the other two time periods are fundamentally less than  $30 \mu\text{gal}$ , except for a few points in Fig. 3b, c, and are considered to be within the error level. The question is why the gravity change is as large as depicted in Fig. 3a. To interpret the reason for the gravity change, we shall discuss and interpret in the next section by presuming that it is attributable to the seasonal water storage.

### 5 Seasonal precipitation model

The observation dates of the four measurement campaigns provide a hint to interpret the reason for the large gravity change in Fig. 3a (Apr 27–May 10, 2007 and Aug 27–Sept 12, 2005): water storage. As described above (such as Table 1), the second measurement campaign was conducted during spring (Apr 27–May 10, 2007), while the other three campaigns were performed in autumn or winter (i.e., Aug 27–Sept 12, 2005, Nov 23–Dec 2, 2007, and Sept 24–Oct 30, 2008). Regarding differences of the second,

third, and fourth campaigns relative to the first campaign, the differences for the time periods of (b) Nov. 23–Dec 2, 2007 and Aug 27–Sept 12, 2005 and (c) Sept 24–Oct 30, 2008 and Aug 27–Sept 12, 2005 appear to be small and do not vary much, perhaps because all three campaigns were made at the same or similar season during which atmospheric conditions were fundamentally identical: the rainfall and water storage in this area do not change greatly from year to year. The gravity difference between the first and second campaigns is particularly large; the observation dates were at two different seasons, which might be the main reason. To confirm that point, we discuss the effects of seasonal precipitation below.

Any surface or ground water mass change must cause a gravity change. During the precipitation season, when the rainfall is greater than the sum of evaporation and runoff, the water height reaches the maximum and the water table saturates in the monsoon. The total water storage in this area increases remarkably. In this case, the gravity observation must be affected by the water storage. However, during the dry season, because the rainfall is less than the evaporation and runoff, and because the water mass does not compensate for the loss, the total water storage in this area is at a low level. Correspondingly, the gravity observation is also certainly affected by the water mass change. Therefore, gravity observations performed during different seasons will show aspects of the annual periodic change.

Irrespective of the rainy season or dry season, the gravity change depends on the relative height of the measurement benchmark. If a measurement benchmark is on the top of a mountain, then the gravity will increase

because the water mass is below the observation point when the water storage increases in the surrounding area. However, if a gravity site is located in a low area and is surrounded by mountains, then the gravity will decrease because the water mass is higher than that of the measurement site. Therefore, precipitation affects gravity, but the gravity change trend (positive or negative) depends on the height of the gravity site relative to the surrounding topography. To estimate the practical precipitation effects in the Dali gravity network, one must consider the precipitation and the surrounding topography carefully.

According to “2005 Climate Bulletin of Dali” and “2007 Climate Bulletin of Dali” [<http://www.dali.gov.cn/dlzwz/5117221703734263808/20110329/250328.html>; [http://dl.xxgk.yn.gov.cn/DL\\_Model/newsview.aspx?id=162675](http://dl.xxgk.yn.gov.cn/DL_Model/newsview.aspx?id=162675)], the yearly accumulated precipitation in Dali area is about 1 m, of which about 90 % of the rainfall concentrates in the rainy season during April–October. The rainfall in April of 2007 is prominent, reaching about 1 m height. The Dali area underwent a dry season lasting from November 2006 to March 2007. Consequently, in reference to the first measurement campaign in Aug–Sept 2005, the second measurement campaign in April–May of 2007 immediately followed the rainy season. It can be expected to be affected strongly by the water storage. Hereinafter, we estimate the precipitation effect on gravity assuming an average water height change from September 2005 to April 2007 in the Dali area.

As described above, to estimate the precipitation effect on gravity, the relative height of the gravity site to the topography should be considered. Figure 1 shows the characteristics of the topographic distribution of the Dali area using  $1' \times 1'$  global topographic data (ETOPO1). Several mountains are higher than 3,000 m in this area, between regions A and B depicted in Fig. 3a. We assume the average height difference of water stored in the aquifer as 0.2–1.0 m for the period from September 2005 to April 2007. Then we use two topographic models (ETOPO1 and ETOPO5-global  $5' \times 5'$ ) to estimate the gravity change of each gravity sites caused by the attraction of the water mass changes, with ignore the effects of load of water mass. We compute the gravity change for each gravity site according to the different water height: 0.2, 0.3, 0.4, 0.5, 0.6, 0.7, 0.8, and 1.0 m.

In practical computation, to ensure the accuracy, the computing area is extended to  $6^\circ \times 6^\circ$  ( $23^\circ\text{N}$ – $29^\circ\text{N}$ ,  $97^\circ\text{E}$ – $103^\circ\text{E}$ ) to eliminate the marginal effects. However, because of the gravitational property that gravitation is proportional to the square of distance, the contribution of a water mass in the near field dominates that from a far field, the computing area of  $6^\circ \times 6^\circ$  is sufficient. The most central computing point is singular, but it might be simply ignored if we take a sufficiently small mesh cell.

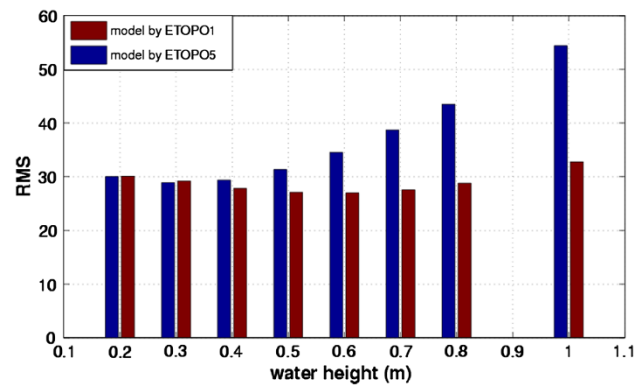


**Fig. 4** RMS comparison of gravity data and the topographic models (ETOPO1 and ETOPO5) using different water storage heights

Using the scheme presented above, we obtained the precipitation effects for different water storage heights. To evaluate the results, we adopted the root mean square (RMS) residuals for different water heights and plotted the RMS results in Fig. 4, which reveals that the ETOPO1 model is better than ETOPO5. The RMS of the ETOPO1 model is about  $26.96 \mu\text{gal}$  at minimum when the water height change of the aquifer is 0.6 m. The correlation between the topographical model and gravity observation is also calculated; results show that the correlation is independent of water mass. It depends only on topography. The correlation coefficient of the ETOPO5 is 0.6; that of ETOPO1 is 0.67. Therefore, ETOPO1 with 0.6 m water change is regarded as the optimum model.

According to the numerical simulation and discussions presented above, a 0.6 m mean water height is assumed for storage from September 2005 to April 2007 in the Dali area (ETOPO1 model). The estimated precipitation effect on gravity is depicted in Fig. 5a: the precipitation effects are fundamentally negative, and reach the maximum gravity change of about  $50 \mu\text{gal}$ , implying that gravity decreases in the whole Dali gravity network because of the seasonal rainfall. This phenomenon is understandable because almost all gravity sites were established along roads which run along rivers or at the foot of mountains, where the terrain height is low. Consequently, the water mass stored in the surrounding mountains is almost always higher than that at the gravity sites, therefore producing negative gravity changes at those gravity sites.

Finally, the gravity change as depicted in Fig. 3a is corrected by subtraction of the precipitation effect, as presented in Fig. 5a. The residual gravity is depicted in Fig. 5b, which shows that the residual gravity is almost less than  $30 \mu\text{gal}$ : the gravity change in Fig. 3a is greatly reduced. Considering the precision of relative gravity measurement, the residual gravity is fundamentally within the  $3\sigma$  error limit. This fact implies that the large gravity change that occurred during September 2005–April 2007 in



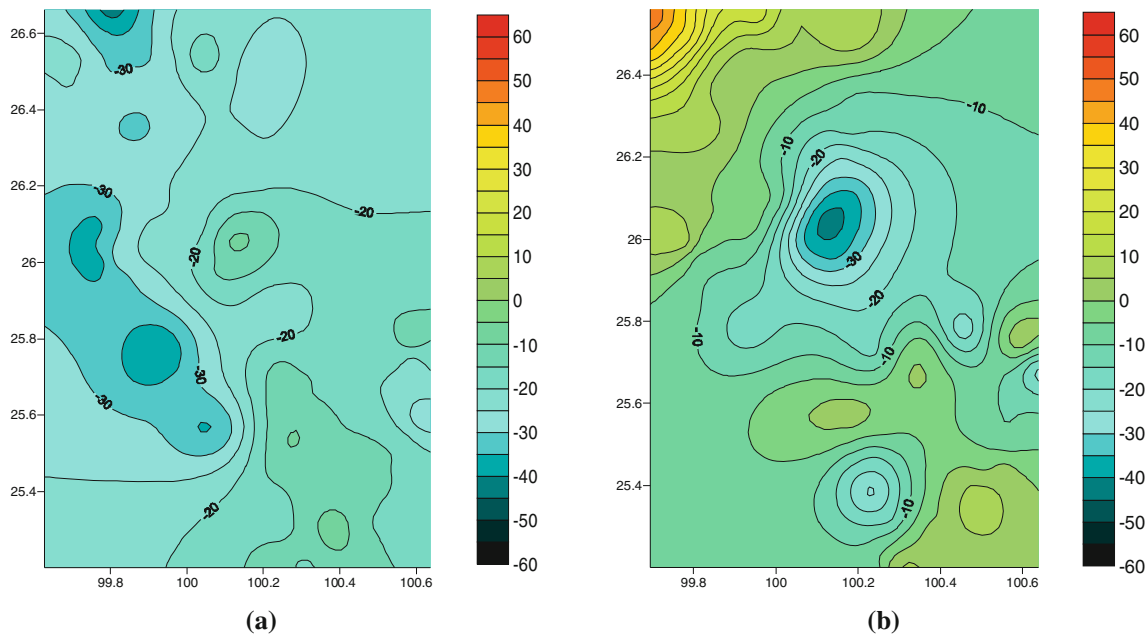


**Fig. 5** Gravity changes during September 2005–April 2007 in the Dali gravity network assuming 0.6 m water height change: **a** modeled precipitation effects–gravity changes; **b** residual gravity after precipitation effect correction. Unit:  $\mu\text{gal}$

the Dali area mainly reflects the precipitation effect. The residual gravity distribution might be considered as the signal of crustal movement, loading effects of rainfall, and observation error. Detail analysis of the residual gravity remains further investigation through modeling.

## 6 Summary and discussions

This study mainly investigated data-processing methods used for the Dali gravity network and interpreted the gravity change caused by seasonal precipitation effect using a mean water storage model. The more absolute gravity data are used in the weighted adjustment, the better the point value accuracy of a relative gravity site is obtained. The calibration function of the LCR relative gravimeter is used as an unknown term. It is obtainable by considering the observed gravity data and the corresponding drift, so that this technique can improve the adjustment accuracy. Final results show that the precision of gravity values obtained for each gravity site is better than  $12 \mu\text{gal}$  if the linear drift coefficient and calibration function is combined in the observation equation. The gravity data obtained at the four absolute gravity stations are used as the constraint datum. Using the data-processing scheme presented above, we processed the gravity data obtained during the four measurement campaigns. We obtained gravity changes in three time periods: Apr–May 2007 and Aug–Sept 2005, Nov–Dec 2007 and Aug–Sept 2005, and

Sept–Oct 2008 and Aug–Sept 2005. Results show that the gravity exhibits a remarkable change in the first time period: Apr–May 2007 and Aug–Sept 2005.

To interpret the large gravity change in the time period of Apr–May 2007 and Aug–Sept 2005 in the Dali gravity network, mean water mass models are assumed for storage in topographic models ETOPO1 and ETOPO5. The precipitation effect on gravity is calculated and compared. Results show that the ETOPO1 topographic model with 0.6 m water height change fits the observed gravity data better, with the correlation factor of 0.67. This fact implies that the precipitation effect is the main cause of gravity change.

It should be pointed out that we used a mean rainfall model instead of real precipitation data in this study. This assumption is acceptable in practice because the contribution of the water storage in the near field (i.e., the water stored in the surrounding mountains) dominates that in a far field. The rainfall amount in the local area can be regarded as the same height. Although more precise precipitation data are expected to improve these results, the water storage rate in the aquifer, which remains unknown, will continue to complicate the accurate estimation of the precipitation effect. Nevertheless, because we considered the rainfall height according to the total amount in the seasons, the model is reasonable. Further investigation of detailed rainfall distribution and storage in the aquifer in the area and the application of the gravity data will be addressed in future studies.

**Acknowledgments** Dr. J. Yu is appreciated for providing the tidal factor. This study was financially supported by the CAS/CAFEA International Partnership Program for creative research teams (No. KZZD-EW-TZ-19) and the National Natural Science Foundation of China (Nos. 41331066 and 41174063).

## References

- Boy JP, Hinderer J (2006) Study of the seasonal gravity signal in superconducting gravimeter data. *J Geodyn* 41:227–233. doi:[10.1016/j.jog.2005.08.035](https://doi.org/10.1016/j.jog.2005.08.035)
- Hao T, Jiang W, Xu Y, Qiu X, Liu J, Dai M, Xu Y, Huang Z, Song H (2005) Geophysical research on deep structure feature in study region of Red River fault zone. *Prog Geophys* 20(3):584–593
- Hwang C, Wang CG, Lee LH (2002) Adjustment of relative gravity measurements using weighted and datum-free constraints. *Comput Geosci* 28(9):1005–1015
- Imanishi Y, Kokubo K, Tatehata H (2006) Effect of underground water on gravity observation at Matsushiro, Japan. *J Geodyn* 41:221–226. doi:[10.1016/j.jog.2005.08.031](https://doi.org/10.1016/j.jog.2005.08.031)
- Jia M, Shao S, Xiang A, Liu D (1995) Gravity effect on water circulation of northwestern Yunnan. *Crustal Deform Earthq* 17(3):340–346
- Kazama T, Okubo S (2009) Hydrological modeling of groundwater disturbances to observed gravity: theory and application to Asama Volcano, Central Japan. *J Geophys Res* 114:B08402. doi:[10.1029/2009JB006391](https://doi.org/10.1029/2009JB006391)
- Leloup PH, Lacassin R, Tapponnier P, Schärer U, Dalai Z, Xiaohan L, Liangshang Z, Shaocheng J, Trinh PT (1995) The Ailao Shan-Red River shear zone (Yunnan, China), Tertiary transform boundary of Indochina: Tectonophysics 251:3–84
- Liu D, Li H, Xing L, Sun S, Liu Z, Xiang A (2007) Analysis of absolute gravimetry result of China earthquake gravity network. *J Geod Geodyn* 27(5):88–93
- Torge W (1989) *Gravimetry*. deGruyter, Berlin, p 465
- Wang Q, Cao X, Ma M (1989) Feature of the recent crustal deformation on the Red-River Fault Zone. *Crustal Deform Earthq* 9(1):1–12
- Xiang H, Guo S, Zhang W, Han Z, Zhang B, Wan J, Dong X, Chen L (2007) Quantitative study of the large scale dextral strike-slip offset in the southern segment of the red river fault since Miocene. *Seismol Geol* 29(1):34–50
- Xing L, Shen C, Li H, Francis O (2009) Comparative observation of absolute gravimeters in Walferdange. *J Geod Geodyn* 29(3):77–79
- Zhao S (1995) Joint inversion of observed gravity and GPS baseline changes for detection of the active fault segment at the Red River fault zone. *Geophys J Int* 122:70–88